Atmospheric Research 176–177 (2016) 267–275

Contents lists available at ScienceDirect

Atmospheric Research

journal homepage: www.elsevier.com/locate/atmosres

Ground-based GNSS network and integrated water vapor mapping during the development of severe storms at the Cuyo region (Argentina)

A. Calori [a,*], J.R. Santos [b], M. Blanco [b], H. Pessano [c,d], P. Llamedo [e], P. Alexander [f], A. de la Torre [e]

[a] Facultad de Ingeniería, Universidad Nacional de Cuyo, Parque General San Martín, Ciudad Universitaria, Mendoza CPM5502JMA, Argentina
[b] Facultad de Ciencias Exactas y Naturales, Universidad de Cuyo, Mendoza CPM5502JMA, Argentina
[c] Facultad Regional San Rafael, Universidad Tecnológica Nacional, Avda. Urquiza 314, San Rafael, Mendoza M5602GCH, Argentina
[d] Dirección de Agricultura y Contingencias Climáticas, Gobierno de Mendoza, San Martín 1850, Mendoza M5560EWS, Argentina
[e] Facultad de Ingeniería, Universidad Austral, Mariano Acosta 191, Pilar, Provincia de Buenos Aires B1629ODT, Argentina
[f] IFIBA, CONICET, Ciudad Universitaria, Buenos Aires C1428EGA, Argentina

ARTICLE INFO

Article history:
Received 10 December 2015
Received in revised form 2 March 2016
Accepted 3 March 2016
Available online 9 March 2016

Keywords:
SIRGAS network
Ground-based GNSS meteorology
IWV mapping
Severe storms

ABSTRACT

Mendoza is a province of Argentina located between 32° S and 34° S at the leeside of the Andes Foothills. Very intense thunderstorms form between October and March (southern hemisphere summer), which produce large hail and damage in crops and properties. Although some hypotheses and conceptual models were proposed in order to identify key possible mechanisms that contribute to trigger convection, they are still waiting for the validation process. As moisture is the main ingredient for storms formation, the identification of its geographical distribution could be used together with other synoptic and mesoscale forcing features to forecast intense convective events. A novel technique in estimating moisture concentration and its geographical distribution has been introduced in order to observe the influx and variability of humidity at this region, during a 45-day period in midsummer. In doing so, we resort to the information provided by the ground-basedGlobal Navigation Satellite System (GNSS) network. More than 300 active stations constitute the continuously operating GNSS network over Southern and Central America (SIRGAS-CON, Sistema de Referencia Geocéntrico para las Américas de Operación Continua). This network allows to retrieve integrated water vapor (IWV) content, mapping this variable by the use of a digital model of terrain. In the period and region under study, a prevailing influx of humidity from N and NE and a high correlation between the accumulation/depletion of humidity and the hail/no hail precipitation days is observed. We discuss in particular the development of five storms detected by the S-Band radar network belonging to the Province of Mendoza. Although the results strongly suggest that IWV maps are capable to represent the humidity dynamics in the considered region, it is still important to highlight that the calculated values for IWV are unrealistic at some locations as the consequence of deep atmospheric gradients. These biases may be explained by the fact that the GNSS observations are made over the whole horizon of each given site.

1. Introduction

The comprehension of the atmospheric circulation is essential to understand the interaction among different spatial and temporal scales. In this context, the South American tropical, subtropical and extratropical atmospheric circulation has been a main subject of study. From satellite images, Virji (1981) settled the general basis of the tropospheric circulation patterns over South America. Successive studies tended to delve into the low-level circulation, some of them focusing on low-level jets (LLJ) (an extensive explanation of LLJ is described by Stensrud, 1996 by the use of radiosonde and pilot balloon observations, models, reanalyses, satellite data, etc. (e.g., Berri and Inzunza, 1993, Nogués-Paegle and Mo, 1997, Saulo et al., 2000, Marengo et al., 2002). The influence of the most important topography features in South America, the Andean Cordillera, over the atmospheric circulation deserves a special mention. The impact that the longest continental mountain range produces on the movements of air masses and precipitation has been investigated and examined in several studies. Among others, Kleeman (1989) examined the implication of the circulation process over the Amazon basin and high Andean plateau, using numerical model simulations, and Garreaud (1999) observed and described the alternation of dry and rainy episodes over the Bolivian Antiplano, at the eastern slope of the mountains, as a consequence of the orography. Saurral et al. (2014) analyzed the impact of varying artificially the altitude of the Andes Cordillera in global climate models and the increase of the model horizontal resolution, to study how these variations determine moisture fluxes and precipitation over some regions of South

* Corresponding author at: Facultad de Ingeniería, Universidad Nacional de Cuyo, Ciudad de Mendoza, Mendoza, Argentina.
E-mail address: acalori@mendoza-conicet.gob.ar (A. Calori).

http://dx.doi.org/10.1016/j.atmosres.2016.03.002
0169-8095/

America. They found a big influence of the location and shape of Andes in the climatology. Different processes related to the Andes mountain range and west–east relief gradient influence the generation of mesoscale circulations that may be affected by surface friction and large-scale pressure gradients, gradually forcing deep moist convection (Nicolini and García Skabar, 2011). These mesoscale circulations are associated with divergence/convergence patterns in the boundary layer over the plains or over complex terrain (Pan et al., 2004, Barthlott et al., 2006, 2010, Kalthoff et al., 2009). The effects of topography in the Central Andes mainly associated with solid precipitation correspond to the persistence of overestimated precipitation using satellite rainfall products, which require a deep assessment (Salio et al., 2015).

The Cuyo region, and within it the province of Mendoza, is located at the semiarid central west part of Argentina (Fig. 1, open box) on the eastern side of the Andean Cordillera and to the south of the subtropical region. Mendoza presents a semiarid climate. The accumulation of moisture and warm fluxes convergence, in addition to the required unstable conditions and an efficient triggering factor, such as upward motion over a frontal zone or diurnal warming and/or orographic lifting (Johns and Doswell, 1992), can produce the most severe events of thunderstorm and hailstorm (e.g., Brooks et al., 2003, García-Ortega et al., 2009). The occurrence of deep convection episodes during the austral warm and moist season (from October until the end of March) strongly affects the cultivated subregions, causing big damages and economic losses. These affected regions are currently protected by an operational hail mitigation project conducted by the Government of Mendoza (www.contingencias.mendoza.gov.ar). This project includes a 4-radar network and an operational silver iodide seeding program by using aircraft and ground-based automatic generators. The social and economical effect of hail precipitation urges for an improvement of the understanding of the different mechanisms involved in the prediction of deep convection (Norte, 1980, Simonelli et al., 2007). In recent years, de la Torre et al. (2004, 2006, 2012, 2015, and references therein-) studied the behavior and influence of mountain wave activity close to the Andes, prior and during the development of tropospheric unstable conditions, as one possible relevant triggering mechanisms for deep convection development in that region of Argentina.

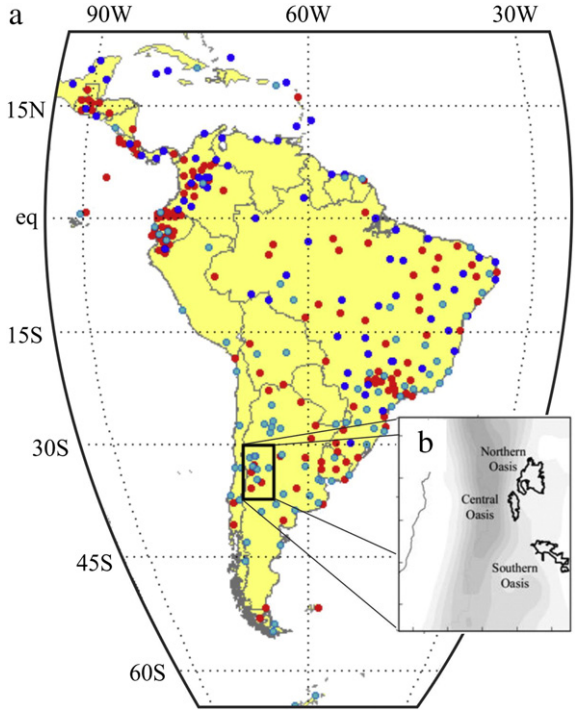

Fig. 1. (a) The SIRGAS-CON network distribution (cyan dots, the SIRGAS-CON-D Sur sites; red dots, the rest of SIRGAS network at march 2010; blue dots, the new SIRGAS sites from 2010 until nowadays). Black box: the Cuyo region. (b) The protected oases. (For interpretation of the references to color in this figure legend, the reader is referred to the web version of this article.)

Within this context, the comprehension of the variability of the influx of water vapor (WV) over Mendoza is of major importance. It could be mostly induced by the southward movement of the Chaco LLJ from northern Argentina (Nicolini and Saulo, 2000, Salio et al., 2002) or from Uruguay, southeast Brazil and the Atlantic Ocean. Teitelbaum et al. (2008) tested several cases and showed an alternative factor of WV, which can produce deep convection over the Mendoza region, related to the eastward motion of the anticyclone at the Pacific Ocean (Jones and Simmonds, 1994). In some cases, after crossing the Andean mountains, the South Pacific anticyclone can deplete or suppress the presence of LLJ with a consequent temperature and humidity decrease (Wang and Fu, 2004). After the anticyclone arrives at the Atlantic coasts, the temperature may increase again and deep convection may reappear over the Mendoza region.

A determination of the amount of atmospheric WV at a given region is not simple. It constitutes a relevant unknown in climatological studies and in weather and contingency prevision. The ground-based GNSS (Global Navigation Satellite System) represents a very promising observatory of the atmosphere (e.g., Duan et al., 1996, Tregoning et al., 1998, Byun and Bar-Server, 2009). The electromagnetic signal from a GNSS satellite suffers a delay through its pass across the neutral atmosphere, partially as result of the presence of WV. The total amount of water vapor present in a vertical atmospheric column over a specific site, like a GNSS site, is called as integrated water vapor (IWV). It is possible to retrieve IWV from that delay, at a level of accuracy equivalent to that expected from direct observational techniques, as radiosondes and microwave radiometers (e.g., Bevis et al., 1992; Rocken et al., 1997). The use of GNSS atmospheric information to study the WV distribution during severe weather events has been already explored in some regions, e.g., Brenot et al. (2006, 2013), during a flash flood and rainfall event in France and Belgium, respectively. Van Baelen et al. (2011) studied the relationship between the WV distribution and precipitation system in Germany. Graham et al. (2012) investigated the mesoscale transport of air and WV from the Swiss lowlands into the Alps, associated with orographic convection and convergence, while de Haan (2013) assimilated WV information into very-short-range regional weather forecasts. Manning et al. (2012) studied an extreme convective super cell storm in Australia using GPS tomography in Australia. In a worldwide context, the application of GNSS for atmospheric remote sensing has a precursor in Europe: the EUMETNET GPS WV (E-GVAP) network. E-GVAP provides ground-based GNSS observations for use in operational meteorology in near real time to be used in numerical weather prevision and weather forecasting (http://www.eumetnet.eu/e-gvap).

In this work, we show the relevance of using IWV maps to draw insight on the accumulation and influx of humidity, previously to the development and occurrence of a series of deep convective processes over Mendoza with intense hail precipitation. These took place during a 45-day interval from the end of December 2009 until mid February 2010. One-hour IWV maps, indentified by the DoY (Day-of-Year) and hour, from SIRGAS tropospheric estimation delay were used.

The data source and map methodology are explained in Section 2 as well as the methodology to retrieve and interpolate IWV in the region of interest. In Section 3, these results are shown for the 45-day period under study, in coincidence with a given number of severe storm developments with and without the simultaneous occurrence of cold fronts. In particular, S-Band radar images and mesoscale model results concerning five storms are discussed. The synoptic conditions, the vertical velocity of air and reflectivity are analyzed in connection with the orographic characteristics. The variability and prevailing direction of humidity influx is discussed in relation to the storm developments. A discussion, some conclusions and a proposed future work are outlined in section 4.

2. Methodology: ground-based GNSS network and IWV mapping

In the context of geodetic techniques, the total effect on the signal of tropospheric refraction (Hogg et al., 1981) is known as the zenith tropospheric delay (ZTD). It is commonly referred to zenith and it must be estimated and computed in order to achieve high geodetic accuracy. The tropospheric composition is constituted mainly by stables gases, nitrogen and oxygen. The dominant component of ZTD is the hydrostatic delay component (ZHD) and can be calculated from the atmospheric pressure. ZTD represents almost 90% of the total delay. The rest of the composition is highly variable, as a consequence of phase changes of atmospheric WV. It is identified as the wet delay (ZWD). Then ZTD = ZHD + ZWD. More than 300 active stations constitute the continuously operating GNSS network over Southern and Central America, namely, the SIRGAS-CON (Sistema de Referencia Geocéntrico para las Américas Continuo) (i.e., Sánchez and Brunini, 2009, Sánchez et al., 2012, 2015) network. Almost 60 stations belong to the global International GNSS Service (IGS) network. SIRGAS-CON represents the densification of the International Terrestrial Reference Frame (ITRF). In this way, the main products of SIRGAS are intended to give an accuracy reference frame over the territory (i.e., loosely constrained weekly solutions, weekly station positions, multi-year solutions). Station position variations between the different SIRGAS realizations are given by a velocity model (Drewes and Heidbach, 2012). In the last 10 years, GNSS observation from SIRGAS have been used in diverse branches of atmospheric research. Free electron distribution studies by means of the Analysis Centre for the Ionosphere (Brunini et al., 2008) contributed to improve the understanding of upper atmosphere processes. The capability of SIRGAS tropospheric estimations for retrieving reliable atmospheric IWV over the territory occupied by this GNSS network is showed by Calori et al. (2014, 2015)—this last hereinafter C15. In these works, an inter-technique comparison was developed. The IWV was compared in terms of ZWD with different sources, which provide this atmospheric information: the water vapor radiometer (WVR) from JASON satellite altimeter mission, reanalysis from the ERA Interim Numerical Model from the European Centre for Medium-Range for Weather Forecast (ECMWF) and IGS tropospheric estimations.

Following the SIRGAS analysis strategy, in agreement with the geodetic standards of the IGS and the International Earth Rotation and Reference Systems Service (IERS), the ZTD was calculated as is described in C15 (an extensive description of SIRGAS analysis strategy for the period of study can be found in Brunini et al., 2012). In this case, 1-h ZTD data from one of the SIRGAS densification networks, the South (SIRGAS-CON-D Sur) (Fig. 1), was used to retrieve IWV (4–10 stations in the study region in 2010 and today, with an average distance of 200 km). For this process, two variables were required from the ERA Interim reanalyses: sea level pressure (SLP) and 2 m temperature (*2 T*). From each ZTD site-dependent value, ZWD was calculated by extracting off ZHD from ZTD, where the former was obtained from the gridded data and spatially and temporally interpolated (0.125° × 0.125° and 00, 06, 12, 18 UT) at each GNSS site.

ZHD is the tropospheric refraction caused by the hydrostatic component of air, expressed in meters. Davis et al. (1985) introduced a modification in the ZHD equation of Saastamoinen (1972), who treated the air as an ideal gas assuming a hydrostatic equilibrium and calculating ZHD with the measured surface pressure (p). The resulting expression is

$$\mathrm{ZHD} = 0.0022768\left(\frac{p}{1-0.00266\cos(2\varnothing)-0.00028\,h.}\right) \quad (1)$$

where h and $\varnothing$ are the height and the latitude of the site, respectively. Due to the lack of surface measurements, the SLP from the ERA Interim model was used. In order to calculate p from SLP, the widely used standard pressure model of Berg (1948) was employed:

$$p = \mathrm{SLP}(1-0.000226\,h)^{5.225} \quad (2)$$

The ZHD calculated from the pressure over the site permitted to extract the wet component of the tropospheric delay, the ZWD. This delay is a consequence of the presence of WV in atmosphere, which causes the other part of the tropospheric refraction on the satellite signal.

The process of retrieving IWV from ZWD needs a critical parameter, the weighted mean temperature (T_m) (Davis et al., 1985). Analogously to p, the temperature must be obtained from the numerical model. Since *2T* is provided with respect to the geopotential level (the orographic height model used by ERA Interim), a height difference correction had to be applied. This was made according to the adiabatic lapse rate. There are several models for calculating T_m. Mendes et al. (2000)

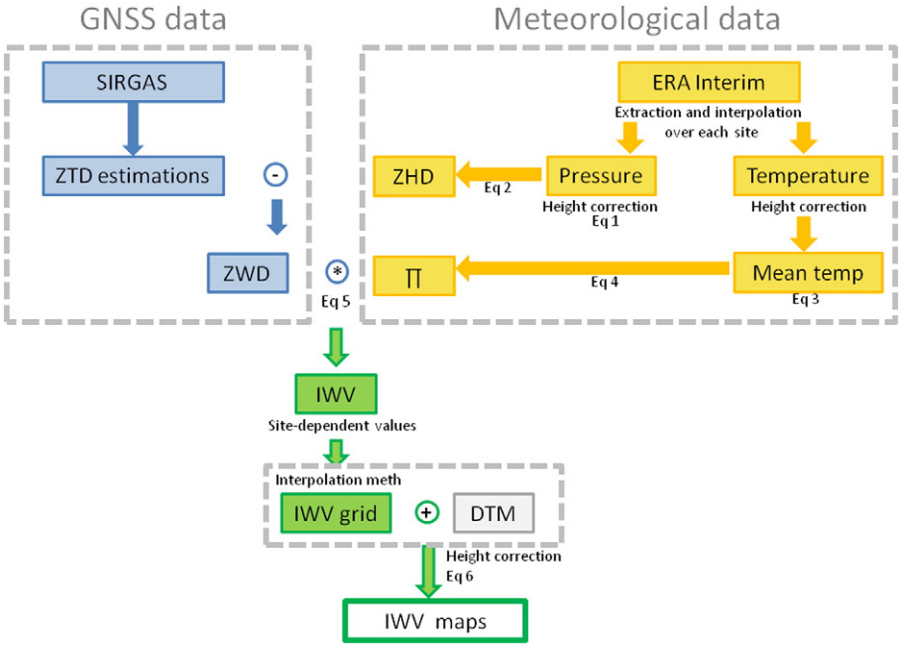

Fig. 2. The process for IWV retrieving and mapping.

made a comparison between seven empirical models of T_m, concluding that these provide identical levels of precision, but different levels of accuracy and that regionally optimized models do not provide superior performance compared to the global models. The model UNB98Tm1 (Eq. 3) was proposed by Mendes (1999) using 50 radiosonde sites and more than 32,500 balloon launches between 62° S to 83° N at different heights (until 2200 m). The expression for the T_m is

$$T_m = 50.4 + 0.789\,T \tag{3}$$

where T is the temperature at the site where the observation is made. The link between ZWD and IWV is given by the dimensionless quantity (Π). It is calculated as

$$\Pi = 10^{-6}\left(K'_2 + \frac{K_3}{T_m}\right) R_W \tag{4}$$

where the refractivity constants are $K_3 = 3.776\,10^5$ and $K'_2 = 16.52$ and R_W is the ratio between the molar gas constant and molar gas of water, equal to 0.46. Finally, IWV is obtained following the relationship expressed in Eq. (5)

$$IWV = \Pi.ZWD \tag{5}$$

In this way, the conversion to IWV is addressed. Once IWV is obtained above each site, the next step is the representation of IWV over the whole territory under study. In order to map IWV, a regular data grid of 0.125° is defined. Using the thin-plate smoothing spline interpolation, IWV at each grid node is computed. This value is then related to the height of each SIRGAS site and the interpolation criteria applied. Although the GNSS network offers a better temporal and spatial coverage than other IWV observational techniques, it is not yet completely representative of the spatial IWV variability induced by the topography. The South American topography is already heterogeneous with huge elevation changes. The introduction of a digital model of terrain is here required because the water vapor usually decreases with height in much the same manner as the total pressure, although much more rapidly (Askne and Nordius, 1987). The total amount of GNSS stations is not enough to cover the total geographic variations of WV distribution. This is the reason we used a digital elevation model (DEM), to compensate the lack of information and in this way, to compute a more realistic value in each node. The Suttle Radar Topography Mission (SRTM) provided by the National Aeronautic and Space Administration (NASA), the German Aerospace Center (DLR) and the Italian Space Agency (ASI) is employed. This provides information on the third dimension (elevation) in the form of a separate DEM (Rabus et al., 2003). This global data of the topographic height have a 30 arc sec (~ 1 km) in latitude and longitude resolution. For the purpose of this work, it is resampled at ~10 km. The introduction of DEM in the IWV grid is made in the following way: (1) A 0.125° regular height grid (RHG) from each height site is generated following the same criteria as with the IWV grid (thin-plate smoothing spline interpolation), (2) the DEM is calculated at the nodes of the RHS grid, and (3) RHG is compared with respect to DEM at each node and the height difference grid (HDG) is calculated. Finally, each IWV value was corrected for the differences of height using the HDG:

$$IWV_{Corr} = IWV_{Orig} \cdot\ e^{-(HDG)/q} \tag{6}$$

where q is equal to 2000 m according to Kouba (2008) and Yao et al. (2015). In Fig. 3, altitude differences between ERA Interim and DEM are detailed. The high range of variability (between −1000 and 1500 m approximately) evidences the necessity of the applied corrections for height differences. Fig. 2 shows the flow diagram of the followed methodology.

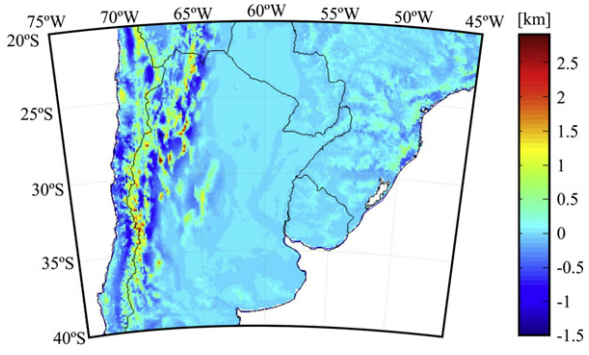

Fig. 3. Altitude differences between ERA Interim and DEM (in km).

3. Application to severe storm developments in the Cuyo region

As a result of the process described in the previous section, IWV maps are achieved. They extend between 20°–40° S and 75°–45° W. Illustratively, in Fig. 4, three representative but different situations are shown (see below). The Cuyo region is deliberately included (black

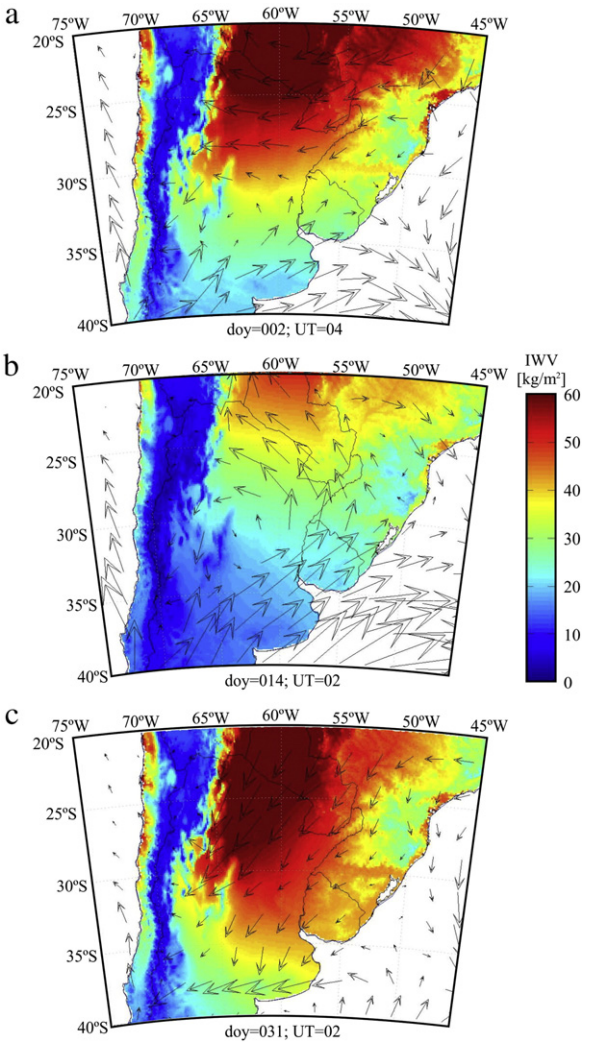

Fig. 4. Three illustrative IWV maps selected from the attached movie described in Section 3 and corresponding to DoY (a) 002, (b) 014 and (c) 031, at 04, 02 and 02 UT, respectively. They show the accumulation and depletion of humidity at the Cuyo region, retrieved from the method here applied as well as wind at 850 hPa from ERA Interim reanalyses. They extend between 20–40 S and 75–45 W.

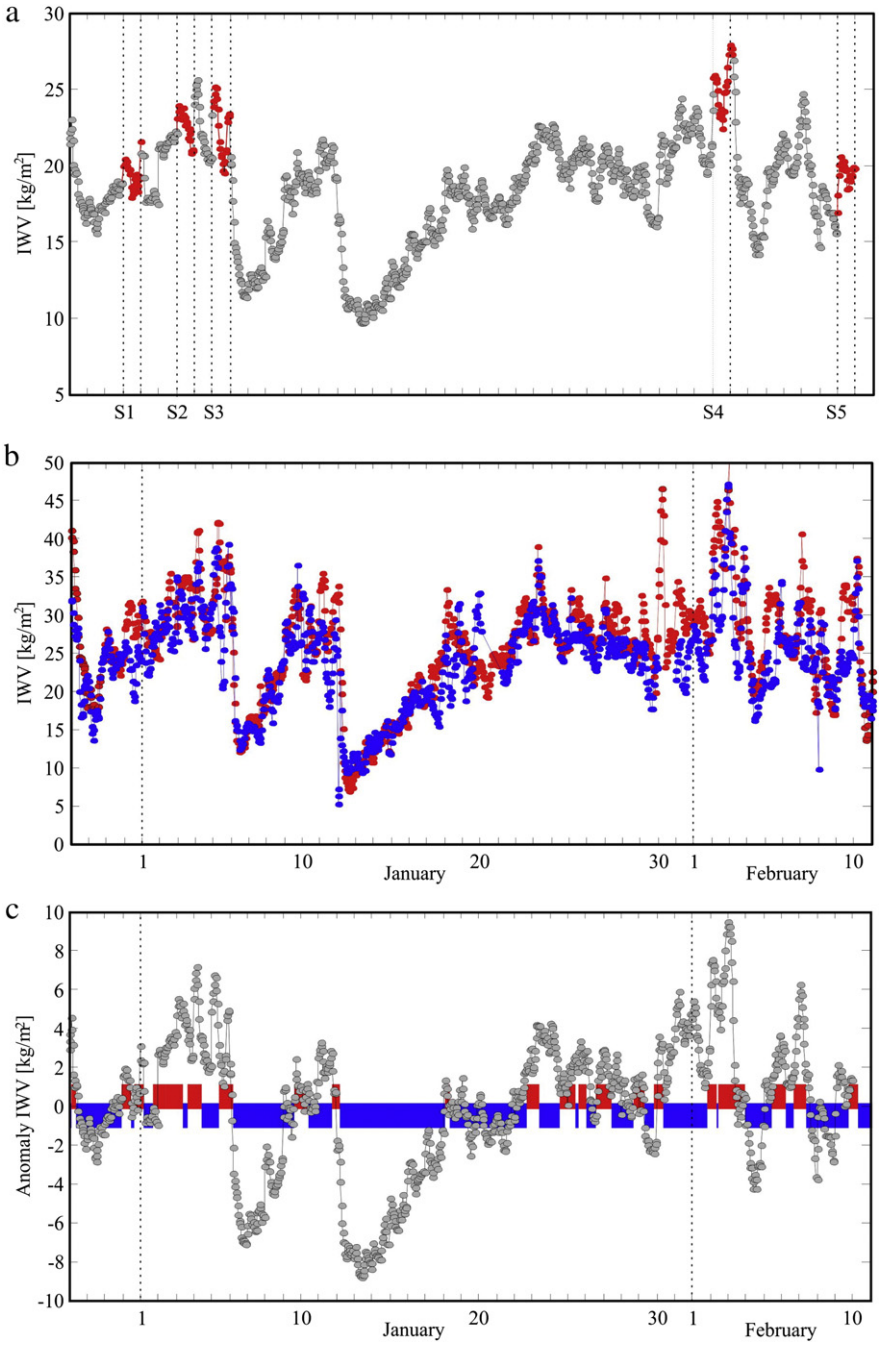

Fig. 5. (a) The variability of IWV at the interpolated mesh point located at 33.4 S, 69.1 W, and altitude = 1000 m. This point was optimally selected close enough to the typical genesis locations above the central oasis. (b) IWV as measured by the two closest GPS stations to the selected mesh point belonging to the SIRGAS network: MZAC and MZAE, in red and blue, respectively. (c) IWV anomalies, after subtracting the mean value. Hail (red) and no hail (blue) precipitation days. (For interpretation of the references to color in this figure legend, the reader is referred to the web version of this article.)

square in Fig. 1) with the aim to understand the humidity flux behavior previously, during and after the development of a succession of severe convective events. We want to test the capability of this technique to provide reliable information about the variability and influx/outflux of humidity in that geographic region. A representative 45-day period was chosen from Dec. 28, 2009 (DoY 360), until Feb. 12, 2010 (DoY 43), during the months with the highest hail precipitation frequency and intensity, following records from the last decade. An animation was generated from the IWV maps, every 2 h from DoYs 360, 2009 until 43, 2010 (see attached movie). In this animation, the wind at 850 hPa was included. Intervals with inflow and accumulation of humidity at the Cuyo region, mostly from N or NE, alternating with drier days where humid sectors are only appreciated at the north of Argentina, may be appreciated.

Within this 45-day period, an almost daily number of deep convection events with significant hail precipitation and surface crop damage were detected (red sectors highlighted in Fig. 5c). We recall that Cuyo is a semiarid region characterized by the presence of three cultivated oases (northern, central and southern, Fig. 1b). A four conventional weather S-Band radar network provides detailed information about the storms generated and/or developed over the subregions under study. In Fig. 5a, the variability of IWV at the interpolated mesh point located at 33.4° S, 69.1° W, and altitude = 1000 m is shown. This point was selected close enough to the typical genesis location above the

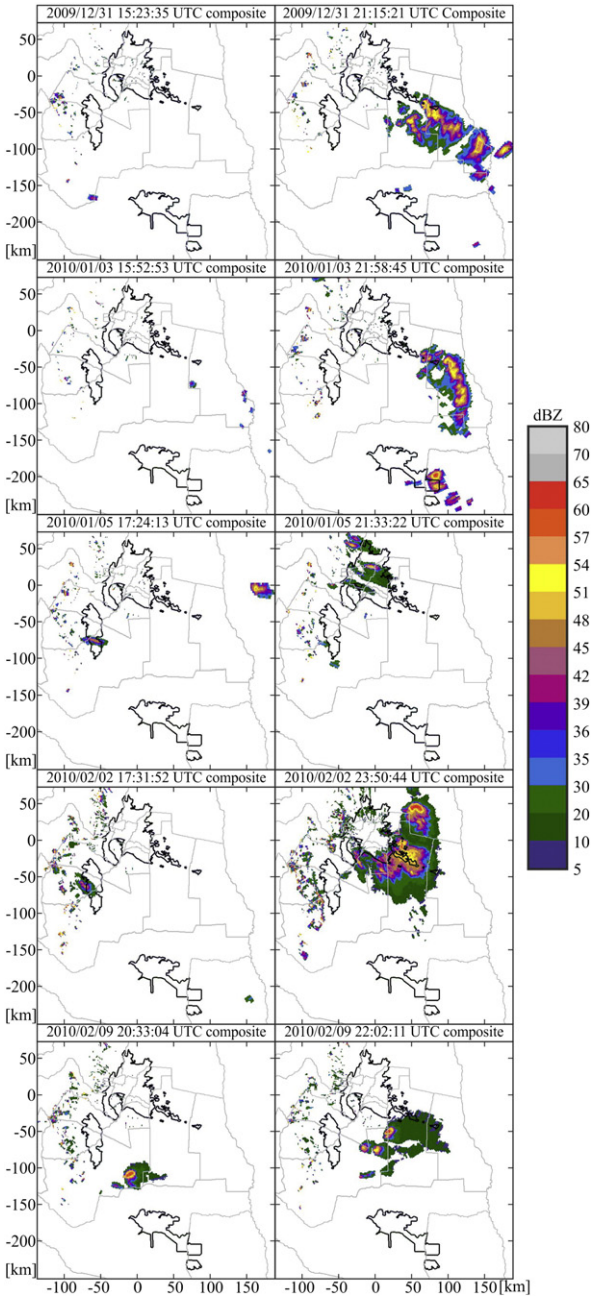

Fig. 6. First S-Band radar echoes (left) and maximum development (right), from top to bottom, respectively, corresponding to the 5 convection events (see text for details) already highlighted in red color in Fig. 5a. (For interpretation of the references to color in this figure legend, the reader is referred to the web version of this article.)

central oasis. The genesis locations have been accurately identified, after 20 years of available and analyzed radar data. They are systematically situated at similar locations above or among the 3 oases (not shown). In Fig. 5b, the IWV variability measured by the two closest GPS stations to the selected mesh point, belonging to the SIRGAS network: MZAC (Mendoza City—approx. 60 km northward) and MZAE (Santa Rosa City—approx. 90 km northeastward). The different scales between Figs. 5a and b are a consequence of the interpolation data and the altitudinal differences: 850 m and 630 m, respectively, against 1000 m at the genesis location. As expected, these curves roughly follow the same variability as in Fig. 5a. To separate positive and negative divergence of humidity, in Fig. 5c, the IWV anomalies are plotted, after subtracting the mean value during the considered period, together with hail (red) and no hail (blue) precipitation periods, according to radar data records. From this figure, as expected, a required condition to be fulfilled for the development of the hail storms is an enough accumulation of humidity at the genesis region. This statement will be analyzed in detail in a future work. The relative importance of the remaining two main ingredients for severe convective storms development, namely, unstable atmospheric conditions and an efficient triggering factor (cold front, mountain waves—see de la Torre et al., 2015 and references therein) clearly define the possible evolution or inhibition of the storm development. This is clear, for example, on days Jan. 31–Feb. 3. In this respect, negative anomalies always correspond to no hail precipitation days. As a rule, if the convective instability and moisture flux convergence conditions are appropriate, convection may be triggered by a combination of factors such as upward motion over a frontal zone or diurnal warming and/or orographic lifting (e.g., Johns and Doswell, 1992). Moist air masses are then pumped from near the ground to their levels of free convection.

The storm events recorded during the considered period have been detected and followed in detail by the S-Band radars mentioned before. The radar data are integrated using the Thunderstorm Identification Tracking Analysis and Nowcasting (TITAN; Dixon and Wiener, 1993) radar software, which provides composite images from the maximum Z values in overlapping areas. The TITAN software defines a storm cell by an operational threshold of 35 dBz and 50 km^3 in volume within a spatial resolution of 1 km^3.

In Fig. 5a, the highlighted red sectors in the curve correspond to five selected storms in particular triggered in the absence of cold fronts and producing considerable hail damage at ground level. Regarding these cases, it may be suspected that the orography played a fundamental role in the triggering of deep convection. These storms constitute a subset from a large number previously considered in de la Torre et al. (2015). The genesis (first radar echoes) and maximum development for these convection events have been recorded from radar data and are shown in Fig. 6. In Fig. 7, the main synoptic features observed from mesoscale numerical simulations that characterize each one of the convective events over the Cuyo region corresponding to Fig. 6, are shown in each panel, respectively, at 12 UTC. They exhibit an increase in the amount of near surface moisture in Cuyo, indicated by high dew point values (greater than 12 °C) and a series of short wave troughs. These waves embedded in the westerly flow in the middle section of the troposphere (500 hPa) provide the forcing mechanism for lifting the air parcels producing intense storms over the Mendoza province. Note that the masking of the topography is done in gray color shading.

4. Discussion and conclusions

As it was mentioned before, our main aim is to propose the application of a recently developed method to observe the IWV evolution during a sequence of severe convective storms above a given geographic region of interest, in this case, the Cuyo region. The constraints and hypotheses involved within Eqs. (1) to (6) are obviously a matter of discussion and possible improvement. Nevertheless, we believe that the potential utility of the method itself may be appreciated through these preliminary results, supported by both radar data and surface damage reports. We believe that these results justify a more detailed analysis in the future, considering a longer period including several years of storm data. From the encouraging correlation observed between damage data at surface level and IWV variability, we may study the seasonal and monthly variability of this correlation. In this context, an insight of the relative importance at this region of IWV accumulation, possible triggering factors and local instability conditions (usually quantified through the convective available potential and convective inhibition indexes) may be relevant. The five events exhibiting similar synoptic conditions were selected just to illustrate the method and were grouped by the presumed influence of the orography as the main triggering mechanism. The SIRGAS-CON network is continuously increasing and the reliability of the results regarding IWV variability too. An improved

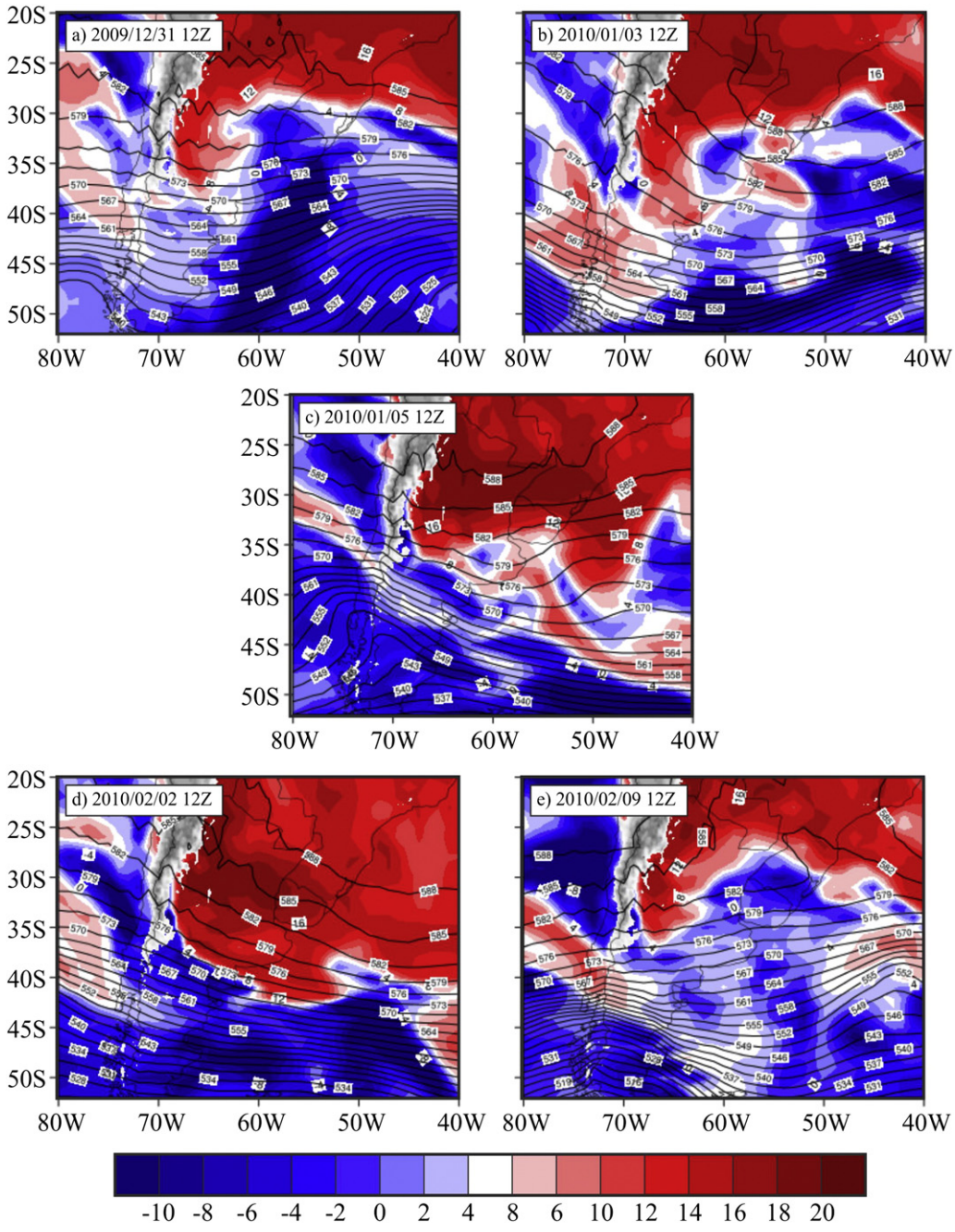

Fig. 7. Dew point (°C) at 850 hPa in shading and geopotential height at 500 hPa.

knowledge of the optimum density of stations to study these mesoscale atmospheric events or even to forecast them on a real time is pending.

In some regions, as for example the north of Chile (Desert of Atacama), calculated values for IWV are unrealistic. This may be seen in Fig. 8, where the average bias for IWV between ERA Interim reanalyses and the method here applied are plotted for the considered period of study. These biases may be explained by the fact that the GNSS observation is always made over the whole horizon of a given site. In locations very close to a very large atmospheric *T* gradient, the GNSS technique, through the method followed to obtain ZTD in this work, is not capable to provide correct atmospheric information over this specific site. The ZTD is obtained from the contributions of the observations at different directions which in turn are highly variable. In the example of Atacama, one of the most arid regions of the planet, this phenomenon can be observed. The data from satellite radiometers

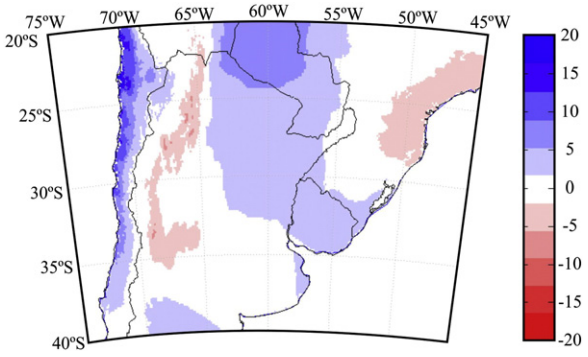

Fig. 8. Average bias for IWV, in kg/m^{-2}, between the method here applied and ERA Interim reanalyses, from the 45-day period considered.

(like Jason1 water vapor radiometer, which was used in C15) permit to see the high variation of WV content over the ocean areas until near the coastline (not shown). The variations range from 30 kg/m^2 in open sea at 100 km from the coast to less than 10 kg/m^2 at 30 km into the continent. This marked tendency to decrease is constant toward the Atacama Desert, where the lowest minimum values of water vapor are recorded. The GNSS site closest to the Atacama Desert is IQQE (at ~100 km northward), in Iquique city, on the coastline. With a good satellite configuration over its horizon, the ZTD from IQQE was obtained from maximum 11 satellites at different elevation heights and azimuths. They were located over the sea, the litoral area or the desert and contributed to the final ZTD. As a result, these values were around 20–30 kg/m^2 (as seen in the maps in Fig. 3 and the animation). In the comparison made by C15, IQQE did not show outlier values with respect to the other SIRGAS sites. A possible reason could be the fact the average value from the radiometer was composed by very variable values, like these from the GNNS technique.

Besides this circumscribed limitation, the GNSS meteorology is promising for monitoring severe weather events. At present, several researchers (Guerova et al., 2013) are developing and improving the methodologies for retrieval and modeling IWV from ground-based GNSS networks. We will direct our future works in this direction, in order to provide a reliable product.

Acknowledgments

Manuscript prepared under grant CONICET PIP 11220090100649 and PICT 1097-2013. A. Calori and M. Blanco are fellows from CONICET. A. de la Torre, P. Llamedo and P. Alexander are members from CONICET. S-Band radar data were provided by the Dirección de Agricultura y Contingencias Climáticas, Goverment of Mendoza.

The authors thank the European Centre for Medium-Range Weather Forecasts (ECMWF) (Dee et al., 2011) for providing the data used in this study, the ECMWF ERA Interim data, which have been obtained from the ECMWF Data Server.

References

Askne, J., Nordius, H., 1987. Estimation of tropospheric delay for microwaves from surface weather data. Radio Sci. 22, 379–386.
Barthlott, C., Corsmeier, C., Meißner, C., Braun, F., Kottmeier, C., 2006. The influence of mesoscale circulation systems on triggering convective cells over complex terrain. Atmos. Res. 81, 150–175.
Barthlott, C., Schipper, J.W., Kalthoff, N., Adler, B., Kottmeier, C., Blyth, A., Mobbs, S., 2010. Model representation of boundary-layer convergence triggering deep convection over complex terrain: a case study from COPS. Atmos. Res. 95, 172–185.
Berg, H., 1948. Allgemeine meteorologie. Dümmler's Verlag, Bonn (in German).
Berri, G., Inzunza, J.B., 1993. The effect of the low-level jet on the poleward water vapour transport in the central region of South America. Atmospheric environment. Part A. General Topics 27, 335–341.
Bevis, M., Businger, S., Herring, T.A., Rocken, C., Anthes, R.A., Ware, R.H., 1992. GPS meteorology: remote sensing of atmospheric water vapor using the global positioning system. J. Geophys. Res. 97 (D14), 15787–15801.
Brenot, H., Ducrocq, V., Walpersdorf, A., Champollion, C., Caumont, O., 2006. GPS zenith delay sensitivity evaluated from high-resolution numerical weather prediction simulations of the 8–9 September 2002 flash flood over southeastern France. J. Geophys. Res. 111 (D15), 105. http://dx.doi.org/10.1029/2004JD005726.
Brenot, H., Neméghaire, J., Delobbe, L., Clerbaux, N., De Meutter, P., Deckmyn, A., Delcloo, A., Frappez, L., Van Roozendael, M., 2013. Preliminary signs of the initiation of deep convection by GNSS. Atmos. Chem. Phys. 13, 5425–5449. http://dx.doi.org/10.5194/acp-13-5425-2013.
Brooks, H.E., Lee, J.W., Craven, J.P., 2003. The spatial distribution of severe thunderstorm and tornado environments from global reanalysis data. Res. 67-68, 73–94.
Brunini, C., Meza, A., Gende, M., Azpilicueta, F., 2008. South American regional maps of vertical TEC computed by GESA: a service for the ionospheric community. Adv, Space Res., Amsterdam 42, 737–744.
Brunini, C., Sánchez, L., Drewes, H., Costa, S., Mackern, V., Martinez, W., Seemüeller, W., Da Silva, A., 2012. Improved analysis strategy and accessibility of the SIRGAS reference frame. In: Kenyon, S., Pacino, M.C., Marti, U. (Eds.), geodesy for planet earth, IAG Symposia V. 136, pp. 3–10.
Byun, S.H., Bar-Server, Y.E., 2009. A new type of troposphere zenith path delay product of the international GNSS service. J. Geod. 83 (3–4), 367–373.
Calori, A., Colosimo, G., Crespi, M., Azpilicueta, F., Gende, M., Brunini, C., Mackern, M.V., 2014. Zenith wet delay retrieval using two different techniques for the South American region and their comparison. In: Rizos, Chris, Willis, Pascal (Eds.), International Association of Geodesy Symposia, Berlin vol. 139, pp. 59–64.
Calori, A., Colosimo, G., Crespi, M., Mackern, M.V., 2015. Comparison of different techniques for retrieving the ZWD over South America and surrounding oceans. In: Sneeuw, N., Novák, P., Crespi, M., Sansò, F. (Eds.), International Association of Geodesy Symposia vol. 142, pp. 1–7.
Davis, J.L., Herring, T.A., Shapiro, I., Rogers, A.E., Elgened, G., 1985. Geodesy by interferometry: effects of atmospheric modeling errors on estimates of base line length. Radio Sci. 20, 1593–1607.
Dee, D.P., Uppala, S.M., Simmons, A.J., et al., 2011. The ERA-Interim reanalysis: configuration and performance of the data assimilation system. Q. J. R. Meteorol. Soc. 137, 553–597. http://dx.doi.org/10.1002/qj.828.
de Haan, S., 2013. Assimilation of GNSS ZTD and radar radial velocity for the benefit of very-short-range regional weather forecasts. Q.J.R. Meteorol. Soc. 139, 2097–2107. http://dx.doi.org/10.1002/qj.2087.
de la Torre, A., Vincent, D., Tailleaux, R., Teitelbaum, H., 2004. A deep convection event above the Tunuyn Valley near to the Andes Mountains. Mon. Weather Rev. 132 (9), 2259–2268.
de la Torre, A., Alexander, P., Llamedo, P., Menéndez, C., Schmidt, T., Wickert, J., 2006. Gravity waves above the Andes detected from GPS radio occultation temperature profiles: jet mechanism? Geophys. Res. Lett. 33, L24810. http://dx.doi.org/10.1029/2006GL027343.
de la Torre, A., Alexander, P., Hierro, R., Llamedo, P., Rolla, A., Schmidt, T., Wickert, J., 2012. Large-amplitude gravity waves above the southern Andes, the Drake Passage, and the Antarctic Peninsula. J. Geophys. Res. 117, D02106. http://dx.doi.org/10.1029/2011JD016377.
de la Torre, A., Pessano, H., Hierro, R., Santos, R., Llamedo, P., Alexander, P., 2015. The influence of topography on vertical velocity of air in relation to severe storms near the Southern Andes Mountains. Atmos. Res.
Dixon, M., Wiener, G., 1993. TITAN: thunderstorm identification, tracking, analysis and nowcasting, a radar-based methodology. J. Atmos. Ocean. Technol. 10, 785–797.
Drewes, H., Heidbach, O., 2012. The 2009 horizontal velocity field for South America and the Caribbean. In: Kenyon, S., Pacino, M.C., Marti, U. (Eds.), Geodesy for Planet Earth, IAG Symposia V 136, pp. 657–664.
Duan, J., Bevis, M., Fang, P., Bock, Y., Chiswell, S., Businger, S., Rocken, C., Solheim, F., van Hove, T., Ware, R., McClusky, S., Herring, T.A., King, R.W., 1996. GPS meteorology: direct estimation of the absolute value of precipitable water. J. Appl. Meteorol. 35, 830–838.
García-Ortega, E., López, L., Sánchez, J.L., 2009. Diagnosis and sensitivity study of two severe storm events in the Southeastern Andes. Atmos. Res. 93, 161–178.
Garreaud, R.D., 1999. Multiscale analysis of the summertime precipitation over the Central Andes. Mon. Weather Rev. 127, 901–921.
Graham, E., Koffi, E., Mätzler, C., 2012. An observational study of air and water vapour convergence over the Bernese Alps, Switzerland, during summertime and the development of isolated thunderstorms. Meteorol. Z. 21 (6), 561–574.
Guerova, G., Jones, J., Dousa, J., Dick, G., de Haan, S., Pottiaux, E., Bock, O., Pacione, R., Elgered, G., Vedel, H., 2013. Advanced Global Navigation Satellite Systems tropospheric products for monitoring severe weather events and climate (GNSS4SWEC). Proceedings of the 4th International Colloquium—Scientific and Fundamental Aspects of the Galileo Programme, Prague, Czech Republic, 4-6.12.
Hogg, D.C., Guiraud, F.O., Sweezy, W.B., 1981. The short-term temporal spectrum of precipitable water vapor. Science 213, 1112–1113.
Johns, R.H., Doswell, C.A.I.I.I., 1992. Severe local storms forecasting. Weather Forecast. 7, 588–612.
Jones, D.A., Simmonds, I., 1994. A climatology of southern hemisphere anticyclones. Clim. Dyn. 10, 333–348.
Kalthoff, N., Adler, B., Barthlott, C., Corsmeier, U., Mobbs, S., Crewell, S., Träumner, K., Kottmeier, C., Wieser, A., Smith, V., 2009. The impact of convergence zones on the initiation of deep convection: a case study from COPS. Atmos. Res. 93, 680–694.
Kleeman, R., 1989. A modeling study of the effect of the Andes on the summertime circulation of tropical South America. J. Atmos. Sci. 46, 3344–3362.
Kouba, J., 2008. Implementation and testing of the gridded Vienna Mapping Function 1 (VMF1). J. Geodyn. http://dx.doi.org/10.1007/s00190-007-0170-3.
Manning, T., Zhang, K., Rohm, W., Choy, S., Hurter, F., 2012. Detecting severe weather in Australia using GPS tomography. J. Global Pos. Syst. 11 (1), 58–70.
Marengo, J.A., Douglas, M.W., Silva Dias, P.L., 2002. The South American low-level jet east of the Andes during the 1999 LBA-TRMM and LBA-WET AMC campaign. J. Geophys. Res. 107 (D20), 8079. http://dx.doi.org/10.1029/2001JD001188.
Mendes, V.B., 1999. Modeling the Neutral-Atmosphere Propagation Delay in Radiometric Space Techniques, (Ph.D. dissertation). Univ. of New Brunswick, Canada.
Mendes, V.B., Prates, G., Santos, L., Langley, R.B., 2000. An evaluation of models for the determination of the weighted mean temperature of the atmosphere, paper presented at Institute of Navigation 2000 National Technical Meeting. Univ. of N. B, Anaheim, Calif.
Nicolini, M., Saulo, A.C., 2000. Eta characterization of the 1997–1998 warm season Chaco jet cases. Preprints 6th International Conference on Southern Hemisphere Meteorology and Oceanography, Chile, pp. 330–331.
Nicolini, M., García Skabar, Y., 2011. Diurnal cycle in convergence patterns in the boundary layer east of the Andes and convection. Atmos. Res. 100 (4), 377–390.
Nogués-Paegle, J., Mo, K., 1997. Alternating wet and dry conditions over South America during summer. Mon. Weather Rev. 125, 279–291.
Norte, F., 1980. Clasificación sinóptica de las tormentas convectivas y su relación con las tareas operativas en el área de defensa. Informe de las primeras experiencias de ajuste de defensa. Temporada granicera 1978–1979. Tomo 2 Pag. 51–95. Programa Nacional de Lucha Antigranizo. Comisión Nacional de Investigaciones Espaciales.
Pan, Z., Arritt, R.W., Takle, E.S., Gutowski Jr., W.J., Anderson, C.J., Segal, M., 2004. Altered hydrologic feedback in a warming climate introduces a "warming hole,". Geophys. Res. Lett. 31, L17109. http://dx.doi.org/10.1029/2004GL020528.

Rabus, B., Eineder, M., Roth, A., Bamler, R., 2003. The shuttle radar topography mission—a new class of digital elevation models acquired by spaceborne radar. ISPRS J. Photogramm. Remote Sens. 57, 241–262.
Rocken, C., Van Hove, T., Ware, R., 1997. Near real-time sensing of atmospheric water vapor. Geophys. Res. Lett. 24, 3221–3224.
Saastamoinen, J., 1972. Contribution to the theory of atmospheric refraction. Bull. Géod. 107, 13–34.
Salio, P., Nicolini, M., Saulo, A.C., 2002. Chaco low-level jet events characterization during the austral summer season. J. Geophys. Res. 107 (D24), 4816.
Salio, P., Hobouchian, M.P., García Skabar, J., Vila, D., 2015. Evaluation of high-resolution satellite precipitation estimates over southern South America using a dense rain gauge network. Atmos. Res. 163, 146–161.
Sánchez, L., Brunini, C., 2009. Achievements and challenges of SIRGAS. In: Drewes, H. (Ed.), Geodetic Reference FramesIAG Symposia Vol. 134. Springer, Heidelberg, pp. 161–166.
Sánchez, L., Seemüller, W., Seitz, M., 2012. Combination of the weekly solutions delivered by the SIRGAS processing centres for the SIRGAS-CON reference frame. In: Kenyon, S., Pacino, M.C., Marti, U. (Eds.), Geodesy for Planet Earth, IAG Symposia 136, pp. 845–851.
Sánchez, L., Drewes, H., Brunini, C., Mackern, M.V., Martínez-Díaz, W., 2015. SIRGAS core network stability. IAG Symposia 143. Springer, Switzerland, pp. 1–8. http://dx.doi.org/10.1007/1345_2015_143.
Saulo, A.C., Nicolini, M., Chou, S.C., 2000. Model characterization of the South American low-level flow during the 1997–1998 spring–summer season. Clim. Dyn. 16, 867–881.
Saurral, R., Camilloni, I., Ambrizzi, T., 2014. Links between topography, moisture fluxes and precipitation over South America. Clim. Dyn. 45, 777–789. http://dx.doi.org/10.1007/s.00382-014-2309-z.
Simonelli, S., Norte, F., Heredia, N., Seluchi, M., 2007. The storm of January 1, 2000, north of the city of Mendoza. Atmosfera 20 (1), 1–23.
Stensrud, D.J., 1996. Effects of persistent, midlatitude mesoscale regions of convection on the large-scale environment during the warm season. J. Atmos. Sci. 53, 3503–3527.
Teitelbaum, H., Le Treut, H., Moustaoui, M., Cabrera, G.C., Ibañez, G., 2008. Deep convection east of the Andes Cordillera: a test case analysis of airmass origin. Mon. Weather Rev. 136, 2201–2209.
Tregoning, P., Boers, R., O'Brien, D., Hendy, M., 1998. Accuracy of absolute precipitable water vapor estimates from GPS observations. J. Geophys. Res. 103.
Van Baelen, J., Reverdy, M., Tridon, F., Labbouz, L., Dick, G., Bender, M., Hagen, M., 2011. On the relationship between water vapour field evolution and the life cycle of precipitation systems. Q. J. R. Meteorol. Soc. 137, 204–223.
Virji, H., 1981. A preliminary study of summertime tropospheric circulation patterns over South America estimated from cloud winds. Mon. Weather Rev. 109, 599–610.
Wang, H., Fu, R., 2004. Influence of cross-Andes flow on the South American low-level jet. J. Clim. 17, 1247–1262.
Yao, Y., Xu, C., Shi, J., Cao, N., Zhang, B., Yang, J., 2015. ITG: a new global GNSS tropospheric correction model. Sci. Report. 5, 10273. http://dx.doi.org/10.1038/srep10273.